Structural Engineering and Mechanics, *Vol. 69, No. 2 (2019) 131-143*
DOI: https://doi.org/10.12989/sem.2019.69.2.131

Nonlinear vibration analysis of the viscoelastic composite nanoplate with three directionally imperfect porous FG core

M. Mohammadi[a] and A. Rastgoo*

School of Mechanical Engineering, College of Engineering, University of Tehran, Tehran, Iran

(Received June 21, 2018, Revised October 2, 2018, Accepted October 3, 2018)

Abstract. In this study, the nonlinear vibration analysis of the composite nanoplate is studied. The composite nanoplate is fabricated by the functional graded (FG) core and lipid face sheets. The material properties in the FG core vary in three directions. The Kelvin-Voigt model is used to study the viscoelastic effect of the lipid layers. By using the Von-Karman assumptions, the nonlinear differential equation of the vibration analysis of the composite nanoplate is obtained. The foundation of the system is modeled by the nonlinear Pasternak foundation. The Bubnov-Galerkin method and the multiple scale method are used to solve the nonlinear differential equation of the composite nanoplate. The free and force vibration analysis of the composite nanoplate are studied. A comparison between the presented results and the reported results is done and good achievement is obtained. The reported results are verified by the results which are obtained by the Runge-Kutta method. The effects of different parameters on the nonlinear vibration frequencies, the primary, the super harmonic and subharmonic resonance cases are investigated. This work will be useful to design the nanosensors with high biocompatibility.

Keywords: three dimensional FG; nonlinear vibration frequency; lipid layers; composite nanoplate

1. Introduction

The biocompatibility is one of the most important factors in the nano and bio sensors. The devices should be compatible with the living tissue. Recently, the researchers used the nanoresonators to predict the proteins (Fischer *et al.* 2008), the attachment of the virus (Ilic *et al.* 2004), DNA molecules (Ilic *et al.* 2005) and prostate-specific antigen (Hwang *et al.* 2004). Lipids are dominant components of membranes. Also, it hosts much of the machinery for cellular communication and transport across the cell membrane. Recently, the researchers fabricated a nanosensor with carbon nanotubes and lipid layer to detect the DNA-damage (Liu *et al.* 2013). The scientists presented a lipid nano transistor which has many potential applications to study the biological process in the cell membranes (Zhou *et al.* 2007). They reported a means of creating nanopores that comprise ultra-short single-walled carbon nanotubes (SWCNTs) inserted into a lipid bilayer. Recent findings show that a high affinity between the lipid tails and the graphene basal plane promoting a favorable hetero-structure for biosensing applications (Lima *et al.* 2016). They reported that the lipids also offered graphene a more uniform and smoother support, reducing graphene hysteresis loop. In order to increase the strength of the structures and decrease the weight of the structures, the FG material can be used. In this class of the material, the properties of the material are different in any point of the structure. Micro-/nano-scaled structures made from functionally graded materials (FGMs) have been proposed as building blocks of micro-/nano-electromechanical systems (MEMS/NEMS) (Fu *et al.* 2004, Witvrouw and Mehta 2005) as well as shape memory alloy and thin films (Bogdanski *et al.* 2002, Sioh 2010). The potential usage of functionally graded nanosensors and nanoactuators is also under investigation. In recent years, the researchers studied the mechanical behavior of the FG nanomaterials (Ebrahimi and Jafari 2018, Hadi *et al.* 2018, Hadi *et al.* 2018). The effect of thermal loading on the mechanical behavior of nanostructures have been investigated (Ebrahimi and Salari 2015, Ebrahimi *et al.* 2015, Ebrahimi and Barati 2016, Ebrahimi and Hosseini 2016, Ebrahimi and Jafari 2016, Ebrahimi and Salari 2016, Ebrahimi and Barati 2017, She *et al.* 2017, She *et al.* 2017, Ebrahimi and Barati 2018). Among of these studies, some researchers utilized the higher order shear deformation theory to investigate the vibration behavior of nanobeam (Ebrahimi and Jafari 2016, Ebrahimi and Farazmandnia 2017). In the most works, the researchers assumed that the FG properties are varied in one direction. But the practical studies showed that the FG properties can be changed in two or three directions. There are a few works that the researchers investigated the mechanical behavior of this kind of FG material (She *et al.* 2017, Zamani Nejad *et al.* 2017, Ashofteh *et al.* 2018, Hadi *et al.* 2018, Hadi *et al.* 2018, Hosseini *et al.* 2018).

To analysis of the mechanical behavior of the nanostructure, the researchers used the size dependent continuum theories. The nonlocal continuum theory (Ebrahimi and Hosseini 2016, Ebrahimi and Barati 2017, Ebrahimi and Dabbagh 2017, She *et al.* 2017, Belmahi *et al.* 2018, Ebrahimi and Barati 2018, Hosseini-Hashemi and Khaniki 2018, Nejad *et al.* 2018), the strain gradient

*Corresponding author, Professor
E-mail: prof.abbass.rastgoo@gmail.com
[a]Ph.D. Candidate

ISSN: 1225-4568 (Print), 1598-6217 (Online)

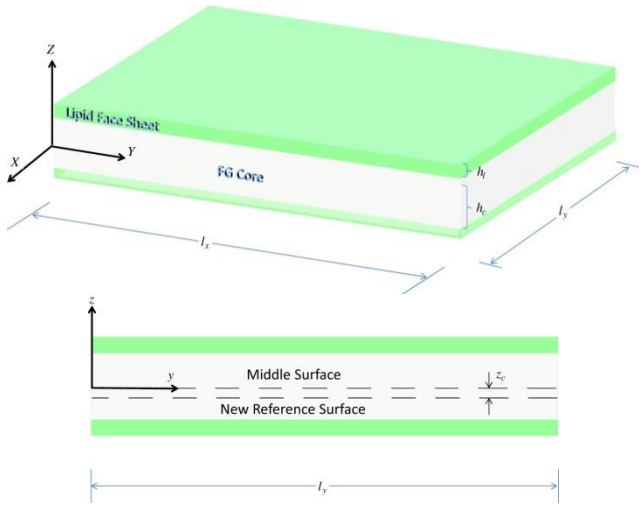

Fig. 1 Isometric and Front view of the composite nanoplate

continuum theory (Ebrahimi *et al.* 2017) and the couple stress continuum theory (Nejad *et al.* 2017, Ajri and Fakhrabadi 2018, Hadi *et al.* 2018) are some of the size dependent continuum theories. Some of these continuum theories show softening or hardening behaviors (Ebrahimi and Barati 2016, Ebrahimi and Barati 2017, Ebrahimi and Barati 2018). Recently, it has been tried to cover both softening and stiffness-hardening behaviors of nanostructures by the means of employing nonlocal strain gradient theory (Ebrahimi and Barati 2016, Ebrahimi and Barati 2017, Ebrahimi *et al.* 2017, Ebrahimi and Dabbagh 2017, Ebrahimi and Barati 2018). Among these theories, the nonlocal continuum theory has been used extensively. This is because the results of this theory are closely with the experimental and simulation results.

In the recent years, the researchers studied the mechanical behavior of the FG nanostructures with porosity distribution types (Ebrahimi and Mokhtari 2015, Ebrahimi and Zia 2015, Ebrahimi *et al.* 2016, Ebrahimi and Jafari 2016, Ebrahimi and Barati 2017). Some researchers presented valuable works to study the effect of the porosity on the mechanical behavior of the nanotubes (She *et al.* 2018, She *et al.* 2018, She *et al.* 2018). In another interesting work, the Timoshenko theory is used to analyze the nonlinear vibration of the nanobeam (Ebrahimi and Zia 2015). In that work, it was explicitly shown that the porosity effect plays important role in the vibration behavior of the nanobeam. The wave propagation analysis for the FG magneto-electro-elastic (MEE) plate was studied in the valuable work (Ebrahimi and Dabbagh 2017). In that work, the authors were used the nonlocal strain gradient theory to capture size effect on the vibration behavior of the nanoplate. Also, they assumed that the MEE properties are varied in the thickness of the nanoplate. The effect of the surface effect on the nonlinear vibration analysis of the nanoplate was investigated (Ebrahimi and Heidari 2017). In that work, the differential quadrature method (DQM) was used to solve the differential governing equation. The buckling behavior of the FG nanobeam was investigated by using the consist couple stress theory (Hadi *et al.* 2018).

To the best author's knowledge, the vibration analysis of three-directionally FG nanoplate has not been studied yet. Also, there is no work that the nonlinear vibration behavior of the composite nanoplate with lipid layers and FG core has been investigated. Besides, the influences of small scale, aspect ratio of the plate, Winkler and Pasternak effects and the viscoelastic coefficient are also discussed. The plots for the ratio of nonlinear to linear frequencies versus maximum transverse amplitude for viscoelastic composite nanoplate are presented. In addition, some new behaviors from the nonlinear vibration are reported in detail. Thus, the differential governing equations are derived in the second section of this paper and the solution method of the governing equations is presented in the third section. Finally, the results of the work are presented in the fourth section.

2. Mathematical modeling

Unlike the classical continuum theory, the advanced continuum theory can predict the size scale in the mechanical analysis of the nanostructures. The size scale in this class of the structures plays important role and the experimental investigations clearly showed this fact. As mentioned in the previous section, the Eringen's continuum theory is used to model the size effect in this work. Among the size-dependent continuum theories, the Eringen's continuum theory is selected because its results are in good achievement with the experimental and simulation results. A complicated form of this theory represents an integral constitutive equation. After some simplification, a differential form of this theory for the constitutive equation has been represented as (Eringen 1983)

$$\sigma_{ij} - \eta\nabla^2\sigma_{ij} = c_{ijkl}\varepsilon_{kl} \tag{1}$$

In the above equation, the parameters σ_{ij} and ε_{kl} are the stress and strain of the composite nanoplate, respectively. Also, the notation η and ∇^2 are defined the nonlocal parameter and the Laplacian operator, respectively. Fig. 1 shows the composite nanoplate with FG core and lipid face sheets.

By considering Eq. (1), the constitutive relations of composite nanoplate are developed as (Farajpour *et al.* 2016)

$$\begin{Bmatrix}\sigma_{xx}\\ \sigma_{yy}\\ \tau_{xy}\end{Bmatrix} - \eta\nabla^2\begin{Bmatrix}\sigma_{xx}\\ \sigma_{yy}\\ \tau_{xy}\end{Bmatrix} = \left(1+\alpha g\frac{\partial}{\partial t}\right)\begin{bmatrix}Q_{11} & Q_{12} & 0\\ Q_{12} & Q_{22} & 0\\ 0 & 0 & Q_{66}\end{bmatrix}\begin{Bmatrix}\varepsilon_{xx}\\ \varepsilon_{yy}\\ 2\varepsilon_{xy}\end{Bmatrix} \tag{2}$$

In the above equations, the parameters $Q_{ij}(i,j=1,2,6)$ and α are defined as

$$\begin{gathered}Q_{11} = Q_{11}^c + Q_{11}^l,\ Q_{12} = Q_{12}^c + Q_{12}^l,\ Q_{22} = Q_{22}^c + Q_{22}^l,\\ Q_{66} = Q_{66}^c + Q_{66}^l,\ \alpha = Q_{11}^l / Q_{11}^c + Q_{11}^l\end{gathered} \tag{3}$$

The elastic constants with superscripts c and l are related to the elastic constants of FG core and lipid layers, respectively. The stiffness of the FG core of the composite nanoplate are demonstrated by the parameters

Q_{ij}^{c} $(i, \mathrm{j}=1,2,6)$ as

$$Q_{11}^{c}=Q_{22}^{c}=\frac{E(x,y,z)}{1-\upsilon^{2}},\ Q_{12}^{c}=Q_{21}^{c}=\frac{\upsilon E(x,y,z)}{1-\upsilon^{2}},\ Q_{66}^{c}=\frac{E(x,y,z)}{2(1+\upsilon)} \tag{4}$$

The parameters $E(z)$ and υ are used to define the Young's modulus and the poison ratio of the FG core, respectively. In this work, it is assumed that the density and the Young's modulus of the FG core vary through three direction of the core. To this end, the material variation can be expressed as

$$P(x,y,z)=\left(1-\gamma V_{p}(x,y)\right)\left((P_{top}-P_{bottom})\left(\frac{z+z_{0}}{h}+\frac{1}{2}\right)^{k}+P_{bottom}\right)$$

$$V_{p}(x,y,z)=\begin{cases}\alpha\sin\left(\dfrac{\pi x}{l_{a}}\right)\cos\left(\dfrac{\pi y}{l_{b}}\right) & \text{I}\\ \alpha\sin\left(\dfrac{\pi x}{l_{a}}\right)\left(1-\cos\left(\dfrac{\pi y}{l_{b}}\right)\right) & \text{II}\end{cases} \tag{5}$$

The notations l_a and l_b are defined the length and the width the FG core, respectively. The z_0 is the distance between the neutral axis and the centroid axis of the composite nanoplate. The power index of material, the material properties of the top and bottom surface composite nanoplate FG core are symbolized by the parameters k, P_{top} and P_{bottom}, respectively. The type I and II are called O and X distribution, respectively. The change of the Young's modulus in the x-y plane is shown in Fig. 2. The parameter α is stated the volume fraction porosity. The strain components are presented in the terms of the displacement components.

$$\varepsilon_{xx}=\varepsilon_{xx}^{0}+z\kappa_{xx},\quad \varepsilon_{yy}=\varepsilon_{yy}^{0}+z\kappa_{yy},\quad \varepsilon_{xy}=\varepsilon_{xy}^{0}+z\kappa_{xy} \tag{6}$$

According to the von Kármán's assumptions and by utilizing the Kirchhoff plate theory, the parameters ε_{ij}^{0} and κ_{ij} $(i,j=x,y)$ are defined as

$$\varepsilon_{xx}^{0}=\frac{\partial u}{\partial x}+\frac{1}{2}\left(\frac{\partial w}{\partial x}\right)^{2},\ \varepsilon_{yy}^{0}=\frac{\partial v}{\partial y}+\frac{1}{2}\left(\frac{\partial w}{\partial y}\right)^{2},$$

$$\varepsilon_{xy}^{0}=\frac{1}{2}\left(\frac{\partial u}{\partial y}+\frac{\partial v}{\partial x}+\frac{\partial w}{\partial x}\frac{\partial w}{\partial y}\right), \tag{7}$$

$$\kappa_{xx}=-\frac{\partial^{2}w}{\partial x^{2}},\quad \kappa_{yy}=-\frac{\partial^{2}w}{\partial y^{2}},\quad \kappa_{xy}=-\frac{\partial^{2}w}{\partial x\partial y}$$

The governing differential equations in terms of the stress resultants can be obtained by the Hamilton's principle. One can obtain the following differential equations as

$$\delta u:\ \frac{\partial N_{xx}}{\partial x}+\frac{\partial N_{xy}}{\partial y}=I_{0}\frac{\partial^{2}u}{\partial t^{2}} \tag{9}$$

$$\delta v:\ \frac{\partial N_{yy}}{\partial y}+\frac{\partial N_{xy}}{\partial x}=I_{0}\frac{\partial^{2}v}{\partial t^{2}} \tag{10}$$

$$\begin{aligned}\delta w:\ &\frac{\partial^{2}M_{xx}}{\partial x^{2}}+2\frac{\partial^{2}M_{xy}}{\partial x\partial y}+\frac{\partial^{2}M_{yy}}{\partial y^{2}}+\frac{\partial}{\partial x}\left(N_{xx}\frac{\partial w}{\partial x}+N_{xy}\frac{\partial w}{\partial y}\right)\\&+\frac{\partial}{\partial y}\left(N_{yy}\frac{\partial w}{\partial y}+N_{xy}\frac{\partial w}{\partial x}\right)+q=I_{0}\frac{\partial^{2}w}{\partial t^{2}}-I_{2}\nabla^{2}\left(\frac{\partial^{2}w}{\partial t^{2}}\right)\end{aligned} \tag{11}$$

The in-plane stress and bending momentum (N_{ij} and M_{ij}) are defined as

$$\begin{aligned}N_{xx}&=\int_{a_2}^{a_1}\sigma_{xx}^{l}dz+\int_{a_0}^{b_0}\sigma_{xx}^{c}dz+\int_{b_1}^{b_2}\sigma_{xx}^{l}dz\\N_{yy}&=\int_{a_2}^{a_1}\sigma_{yy}^{l}dz+\int_{a_0}^{b_0}\sigma_{yy}^{c}dz+\int_{b_1}^{b_2}\sigma_{yy}^{l}dz\\N_{xy}&=\int_{a_2}^{a_1}\sigma_{xy}^{l}dz+\int_{a_0}^{b_0}\sigma_{xy}^{c}dz+\int_{b_1}^{b_2}\sigma_{xy}^{l}dz\\M_{xx}&=\int_{a_2}^{a_1}\sigma_{xx}^{l}zdz+\int_{a_0}^{b_0}\sigma_{xx}^{c}zdz+\int_{b_1}^{b_2}\sigma_{xx}^{l}zdz\\M_{yy}&=\int_{a_2}^{a_1}\sigma_{yy}^{l}zdz+\int_{a_0}^{b_0}\sigma_{yy}^{c}zdz+\int_{b_1}^{b_2}\sigma_{yy}^{l}zdz\\M_{xy}&=\int_{a_2}^{a_1}\sigma_{xy}^{l}zdz+\int_{a_0}^{b_0}\sigma_{xy}^{c}zdz+\int_{b_1}^{b_2}\sigma_{xy}^{l}zdz\end{aligned} \tag{12}$$

As Eq. (2) is substituted into Eq. (12), the stress resultants are obtained as

$$\begin{aligned}&N_{xx}-\eta\nabla^{2}N_{xx}=A_{11}\left[\frac{\partial u}{\partial x}+\frac{1}{2}\left(\frac{\partial w}{\partial x}\right)^{2}\right]+A_{11}\left[\frac{\partial v}{\partial y}+\frac{1}{2}\left(\frac{\partial w}{\partial y}\right)^{2}\right]\\&-B_{11}\frac{\partial^{2}w}{\partial x^{2}}-B_{12}\frac{\partial^{2}w}{\partial y^{2}}+\tilde{A}_{11}\left[\frac{\partial^{2}u}{\partial x\partial t}+\frac{\partial w}{\partial x}\frac{\partial^{2}w}{\partial x\partial t}\right]\\&+\tilde{A}_{12}\left[\frac{\partial^{2}v}{\partial y\partial t}+\frac{\partial w}{\partial y}\frac{\partial^{2}w}{\partial y\partial t}\right]-\tilde{B}_{11}\frac{\partial^{3}w}{\partial x^{2}\partial t}-\tilde{B}_{12}\frac{\partial^{2}w}{\partial y^{2}\partial t},\\&N_{yy}-\eta\nabla^{2}N_{yy}=A_{12}\left[\frac{\partial u}{\partial x}+\frac{1}{2}\left(\frac{\partial w}{\partial x}\right)^{2}\right]+A_{22}\left[\frac{\partial v}{\partial y}+\frac{1}{2}\left(\frac{\partial w}{\partial y}\right)^{2}\right]\\&-B_{12}\frac{\partial^{2}w}{\partial x^{2}}-B_{22}\frac{\partial^{2}w}{\partial y^{2}}+\tilde{A}_{12}\left[\frac{\partial^{2}u}{\partial x\partial t}+\frac{\partial w}{\partial x}\frac{\partial^{2}w}{\partial x\partial t}\right]\\&+\tilde{A}_{22}\left[\frac{\partial^{2}v}{\partial y\partial t}+\frac{\partial w}{\partial y}\frac{\partial^{2}w}{\partial y\partial t}\right]-\tilde{B}_{12}\frac{\partial^{3}w}{\partial x^{2}\partial t}-\tilde{B}_{22}\frac{\partial^{2}w}{\partial y^{2}\partial t},\\&N_{xy}-\eta\nabla^{2}N_{xy}=A_{66}\left(\frac{\partial u}{\partial y}+\frac{\partial v}{\partial x}+\frac{\partial w}{\partial x}\frac{\partial w}{\partial y}\right)-2B_{66}\frac{\partial^{2}w}{\partial x\partial y}\\&+\tilde{A}_{66}\left(\frac{\partial^{2}u}{\partial y\partial t}+\frac{\partial^{2}v}{\partial x\partial t}+\frac{\partial^{2}w}{\partial x\partial t}\frac{\partial w}{\partial y}+\frac{\partial^{2}w}{\partial y\partial t}\frac{\partial w}{\partial x}\right)-2\tilde{B}_{66}\frac{\partial^{2}w}{\partial x\partial y\partial t}\end{aligned} \tag{13}$$

$$\begin{aligned}&M_{xx}-\eta\nabla^{2}M_{xx}=B_{11}\left(\frac{\partial u}{\partial x}+\frac{1}{2}\left(\frac{\partial w}{\partial x}\right)^{2}\right)+B_{12}\left(\frac{\partial v}{\partial y}+\frac{1}{2}\left(\frac{\partial w}{\partial y}\right)^{2}\right)\\&-D_{11}\frac{\partial^{2}w}{\partial x^{2}}-D_{12}\frac{\partial^{2}w}{\partial y^{2}}+\tilde{B}_{11}\left(\frac{\partial^{2}u}{\partial x\partial t}+\frac{\partial w}{\partial x}\frac{\partial^{2}w}{\partial x\partial t}\right)\\&+\tilde{B}_{12}\left(\frac{\partial^{2}v}{\partial y\partial t}+\frac{\partial w}{\partial y}\frac{\partial^{2}w}{\partial y\partial t}\right)-\tilde{D}_{11}\frac{\partial^{3}w}{\partial x^{2}\partial t}-\tilde{D}_{12}\frac{\partial^{3}w}{\partial y^{2}\partial t},\\&M_{yy}-\eta\nabla^{2}M_{yy}=B_{12}\left(\frac{\partial u}{\partial x}+\frac{1}{2}\left(\frac{\partial w}{\partial x}\right)^{2}\right)+B_{22}\left(\frac{\partial v}{\partial y}+\frac{1}{2}\left(\frac{\partial w}{\partial y}\right)^{2}\right)\\&-D_{12}\frac{\partial^{2}w}{\partial x^{2}}+\tilde{B}_{12}\left(\frac{\partial^{2}u}{\partial x\partial t}+\frac{\partial w}{\partial x}\frac{\partial^{2}w}{\partial x\partial t}\right)+\tilde{B}_{22}\left(\frac{\partial^{2}v}{\partial y\partial t}+\frac{\partial w}{\partial y}\frac{\partial^{2}w}{\partial y\partial t}\right)\\&-D_{22}\frac{\partial^{2}w}{\partial y^{2}}-\tilde{D}_{12}\frac{\partial^{3}w}{\partial x^{2}\partial t}-\tilde{D}_{22}\frac{\partial^{3}w}{\partial y^{2}\partial t},\\&M_{xy}-\eta\nabla^{2}M_{xy}=B_{66}\left(\frac{\partial u}{\partial y}+\frac{\partial v}{\partial x}+\frac{\partial w}{\partial x}\frac{\partial w}{\partial y}\right)-2D_{66}\frac{\partial^{2}w}{\partial x\partial y}\\&+\tilde{B}_{66}\left(\frac{\partial^{2}u}{\partial y\partial t}+\frac{\partial^{2}v}{\partial x\partial t}+\frac{\partial^{2}w}{\partial x\partial t}\frac{\partial w}{\partial y}+\frac{\partial^{2}w}{\partial y\partial t}\frac{\partial w}{\partial x}\right)-2\tilde{D}_{66}\frac{\partial^{2}w}{\partial x\partial y\partial t}\end{aligned} \tag{14}$$

The new constants in the above equations are defined as

$$\left\langle A_{11},A_{22},A_{12},A_{66}\right\rangle=\int_{a_2}^{a_1}\left\langle Q_{11}^{l},Q_{22}^{l},Q_{12}^{l},Q_{66}^{l}\right\rangle dz+\int_{a_0}^{b_0}\left\langle Q_{11}^{c},Q_{22}^{c},Q_{12}^{c},Q_{66}^{c}\right\rangle dz$$
$$+\int_{b_1}^{b_2}\left\langle Q_{11}^{l},Q_{22}^{l},Q_{12}^{l},Q_{66}^{l}\right\rangle dz$$
$$\left\langle B_{11},B_{22},B_{12},B_{66}\right\rangle=\int_{a_2}^{a_1}\left\langle Q_{11}^{l},Q_{22}^{l},Q_{12}^{l},Q_{66}^{l}\right\rangle zdz$$
$$+\int_{a_0}^{b_0}\left\langle Q_{11}^{c},Q_{22}^{c},Q_{12}^{c},Q_{66}^{c}\right\rangle zdz+\int_{b_1}^{b_2}\left\langle Q_{11}^{l},Q_{22}^{l},Q_{12}^{l},Q_{66}^{l}\right\rangle zdz$$
$$\left\langle D_{11},D_{22},D_{12},D_{66}\right\rangle=\int_{a_2}^{a_1}\left\langle Q_{11}^{l},Q_{22}^{l},Q_{12}^{l},Q_{66}^{l}\right\rangle z^2dz$$
$$+\int_{a_0}^{b_0}\left\langle Q_{11}^{c},Q_{22}^{c},Q_{12}^{c},Q_{66}^{c}\right\rangle z^2dz+\int_{b_1}^{b_2}\left\langle Q_{11}^{l},Q_{22}^{l},Q_{12}^{l},Q_{66}^{l}\right\rangle z^2dz$$
$$\left\langle \tilde{A}_{11},\tilde{A}_{22},\tilde{A}_{12},\tilde{A}_{66}\right\rangle=\int_{a_2}^{a_1}\alpha g\left\langle Q_{11},Q_{22},Q_{12},Q_{66}\right\rangle dz \tag{15}$$
$$+\int_{b_1}^{b_2}\alpha g\left\langle Q_{11},Q_{22},Q_{12},Q_{66}\right\rangle dz,$$
$$\left\langle \tilde{B}_{11},\tilde{B}_{22},\tilde{B}_{12},\tilde{B}_{66}\right\rangle=\int_{a_2}^{a_1}\alpha g\left\langle Q_{11},Q_{22},Q_{12},Q_{66}\right\rangle zdz$$
$$+\int_{b_1}^{b_2}\alpha g\left\langle Q_{11},Q_{22},Q_{12},Q_{66}\right\rangle zdz,$$
$$\left\langle \tilde{D}_{11},\tilde{D}_{22},\tilde{D}_{12},\tilde{D}_{66}\right\rangle=\int_{a_2}^{a_1}\alpha g\left\langle Q_{11},Q_{22},Q_{12},Q_{66}\right\rangle z^2dz$$
$$+\int_{b_1}^{b_2}\alpha g\left\langle Q_{11},Q_{22},Q_{12},Q_{66}\right\rangle z^2dz,$$

In the above constants, the parameters $A_{ij}(i,j=1,2)$, $B_{ij}(i,j=1,2)$ and $D_{ij}(i,j=1,2)$ are related to whole of the composite nanoplate. Applying Eq. (13), one can obtain the mid-plane strains from Eq. (2), as follows

$$\left(1+\alpha g\frac{\partial}{\partial t}\right)\begin{Bmatrix}\varepsilon_{xx}^{0}\\ \varepsilon_{yy}^{0}\\ 2\varepsilon_{xy}^{0}\end{Bmatrix}=\begin{bmatrix}A_{11}^{-1} & A_{12}^{-1} & 0\\ A_{12}^{-1} & A_{22}^{-1} & 0\\ 0 & 0 & A_{66}^{-1}\end{bmatrix}\left(L_{nl}\begin{Bmatrix}N_{xx}\\ N_{yy}\\ N_{xy}\end{Bmatrix}\right) \tag{16}$$

The operator $L_{nl}(*)=(*)-\eta\nabla^2(*)$ is the nonlocal operator. Further, the components $[A_{ij}^{-1}]$ represent the inverse of stretching stiffness matrix $[A_{ij}]$. As Eq. (16) is substituted into Eq. (8), we have

$$L_{nl}\left[A_{11}^{-1}\frac{\partial^2 N_{xx}}{\partial y^2}+A_{12}^{-1}\left(\frac{\partial^2 N_{xx}}{\partial x^2}+\frac{\partial^2 N_{yy}}{\partial y^2}\right)-A_{66}^{-1}\frac{\partial^2 N_{xy}}{\partial x\partial y}+A_{22}^{-1}\frac{\partial^2 N_{yy}}{\partial x^2}\right]$$
$$=\left(1+\alpha g\frac{\partial}{\partial t}\right)\left[\left(\frac{\partial^2 w}{\partial x\partial y}\right)^2-\frac{\partial^2 w}{\partial x^2}\frac{\partial^2 w}{\partial y^2}\right] \tag{17}$$

In this work, the nonlocal compatibility equation of the nano composite nanoplate is presented in Eq. (17). The nonlocal stress resultants, which are used in the above equation, are defined by the Airy's function as

$$N_{xx}=\frac{\partial^2\Theta}{\partial y^2},\quad N_{yy}=\frac{\partial^2\Theta}{\partial x^2},\quad N_{xy}=-\frac{\partial^2\Theta}{\partial x\partial y} \tag{18}$$

By considering this point, the in-plane inertias in Eq. (9) and Eq. (10) are set to zero and these two equations will be

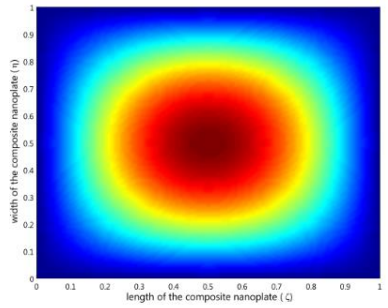

(a)

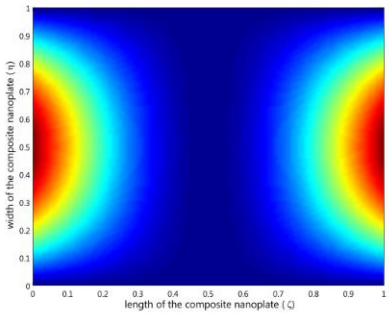

(b)

Fig. 1 The Young modulus distribution FG material composite nanoplate (a) O distribution type (b) X distribution type

exactly satisfied. The external transverse is related to the elastic medium (q_e) and the harmonic external load (q_h). These forces can be expressed as

$$q_h=\bar{F}\cos(\Omega t)\ ,\ q_e=k_l w-k_s\left(\frac{\partial^2 w}{\partial x^2}+\frac{\partial^2 w}{\partial y^2}\right)+k_{nl}w^3 \tag{19}$$

To obtain the nonlinear differential governing equation, some non-dimensional parameters are introduced as

$$\zeta=\frac{x}{l_x},\ \eta=\frac{y}{l_y},\ W=\frac{w}{h},\ \bar{\Theta}=\frac{\Theta}{D_{11}h^2},\ \hat{t}=\frac{t}{l_x^2}\sqrt{\frac{D_{11}}{I_0}},$$
$$\hat{\alpha}=\frac{\alpha g}{l_x^2}\sqrt{\frac{D_{11}}{I_0}},K_s=\frac{k_s l_x^2}{D_{11}},\beta=\frac{l_x}{l_y},\lambda=\frac{l_x}{h},\bar{I}_0=\frac{I_0}{I_0},$$
$$\bar{I}_2=\frac{I_2}{I_0 l_x^2},\chi=\frac{\sqrt{\eta}}{l_x},\bar{u}=\frac{u}{h},\ \bar{v}=\frac{v}{h},\ K_l=\frac{k_l l_x^4}{D_{11}},$$
$$\left\langle A_{11}^{*},A_{12}^{*},A_{66}^{*},A_{22}^{*}\right\rangle=\left\langle\frac{A_{11}^{-1}D_{11}}{h^2},\frac{A_{12}^{-1}D_{11}}{h^2},\frac{A_{66}^{-1}D_{11}}{h^2},\frac{A_{22}^{-1}D_{11}}{h^2}\right\rangle,$$
$$\left\langle \bar{B}_{11},\bar{B}_{12},\bar{B}_{66},\bar{B}_{22}\right\rangle=\left\langle\frac{B_{11}}{D_{11}},\frac{B_{12}}{D_{11}},\frac{B_{66}}{D_{11}},\frac{B_{22}}{D_{11}}\right\rangle,K_{nl}=\frac{k_{nl}l_x^4h^2}{D_{11}}, \tag{20}$$
$$\left\langle \bar{D}_{11},\bar{D}_{12},\bar{D}_{66},\bar{D}_{22}\right\rangle=\left\langle\frac{D_{11}}{D_{11}},\frac{D_{12}}{D_{11}},\frac{D_{66}}{D_{11}},\frac{D_{22}}{D_{11}}\right\rangle,$$
$$\left\langle \bar{B}_{11},\bar{B}_{12},\bar{B}_{66},\bar{B}_{22}\right\rangle=\left\langle\frac{B_{11}}{D_{11}},\frac{B_{12}}{D_{11}},\frac{B_{66}}{D_{11}},\frac{B_{22}}{D_{11}}\right\rangle,K_{nl}=\frac{k_{nl}l_x^4h^2}{D_{11}},$$
$$\left\langle \bar{D}_{11},\bar{D}_{12},\bar{D}_{66},\bar{D}_{22}\right\rangle=\left\langle\frac{D_{11}}{D_{11}},\frac{D_{12}}{D_{11}},\frac{D_{66}}{D_{11}},\frac{D_{22}}{D_{11}}\right\rangle,$$
$$\left\langle \bar{B}_{11}^{*},\bar{B}_{12}^{*},\bar{B}_{66}^{*},\bar{B}_{22}^{*}\right\rangle=\left\langle\frac{\tilde{B}_{11}h}{l_x^2\sqrt{D_{11}I_0}},\frac{\tilde{B}_{12}h}{l_x^2\sqrt{D_{11}I_0}},\frac{\tilde{B}_{66}h}{l_x^2\sqrt{D_{11}I_0}},\frac{\tilde{B}_{22}h}{l_x^2\sqrt{D_{11}I_0}}\right\rangle$$

The nonlocal governing differential equations of the composite nanoplate are obtained by inserting Eqs. (13), (14) and (18) in Eqs. (9)-(11) and Eq. (17). By using the non-dimensional parameters which are defined in Eq. (20), the nonlocal nonlinear differential governing equations in the non-dimensional form can be obtained as

$$
\begin{aligned}
&-\bar{D}_{11}\frac{\partial^4 W}{\partial\zeta^4}-\frac{\partial^2\bar{D}_{11}}{\partial\zeta^2}\frac{\partial^2 W}{\partial\zeta^2}-2\frac{\partial\bar{D}_{11}}{\partial\zeta}\frac{\partial^3 W}{\partial\zeta^3}-\beta^4\left(\begin{array}{l}\bar{D}_{22}\frac{\partial^4 W}{\partial\eta^4}+2\frac{\partial\bar{D}_{22}}{\partial\eta}\frac{\partial^3 W}{\partial\eta^3}\\+\frac{\partial^2\bar{D}_{22}}{\partial\eta^2}\frac{\partial^2 W}{\partial\eta^2}\end{array}\right)\\
&-\beta^2\left(\begin{array}{l}2\bar{D}_{12}\frac{\partial^4 W}{\partial\zeta^2\partial\eta^2}+\frac{\partial^2\bar{D}_{12}}{\partial\zeta^2}\frac{\partial^2 W}{\partial\eta^2}+2\frac{\partial\bar{D}_{12}}{\partial\zeta}\frac{\partial^3 W}{\partial\zeta\partial\eta^2}\\+\frac{\partial^2\bar{D}_{12}}{\partial\eta^2}\frac{\partial^2 W}{\partial\zeta^2}+2\frac{\partial\bar{D}_{12}}{\partial\eta}\frac{\partial^3 W}{\partial\eta\partial\zeta^2}\end{array}\right)\\
&-4\beta^2\left(\begin{array}{l}\bar{D}_{66}\frac{\partial^4 W}{\partial\zeta^2\partial\eta^2}+\frac{\partial^2\bar{D}_{66}}{\partial\zeta\partial\eta}\frac{\partial^2 W}{\partial\zeta\partial\eta}\\+\frac{\partial\bar{D}_{66}}{\partial\zeta}\frac{\partial^3 W}{\partial\zeta\partial\eta^2}+\frac{\partial\bar{D}_{66}}{\partial\eta}\frac{\partial^3 W}{\partial\eta\partial\zeta^2}\end{array}\right)\\
&-\bar{D}_{11}^*\frac{\partial^5 W}{\partial\zeta^4\partial\tau}-2\left(\bar{D}_{12}^*+2\bar{D}_{66}^*\right)\beta^2\frac{\partial^5 W}{\partial\zeta^2\partial\eta^2\partial\tau}-\bar{D}_{22}^*\beta^4\frac{\partial^5 W}{\partial\eta^4\partial\tau}\\
&+4\left(\bar{B}_{12}^*+\bar{B}_{66}^*\right)\beta^2\left(\frac{\partial^3 W}{\partial\zeta\partial\eta\partial\tau}\frac{\partial^2 W}{\partial\zeta\partial\eta}\right)+\bar{B}_{11}^*\left(\begin{array}{l}\frac{\partial^3 W}{\partial\zeta^3}\frac{\partial^2 W}{\partial\zeta\partial\tau}+2\frac{\partial^2 W}{\partial\zeta^2}\frac{\partial^3 W}{\partial\zeta^2\partial\tau}\\+\frac{\partial W}{\partial\zeta}\frac{\partial^4 W}{\partial\zeta^3\partial\tau}\end{array}\right)\\
&+\beta^4\left(\begin{array}{l}\bar{B}_{22}\left(\left(\frac{\partial^2 W}{\partial\eta^2}\right)^2+\frac{\partial W}{\partial\eta}\frac{\partial^3 W}{\partial\eta^3}\right)+\left(\begin{array}{l}\frac{1}{2}\frac{\partial^2\bar{B}_{22}}{\partial\eta^2}\left(\frac{\partial W}{\partial\eta}\right)^2\\+2\frac{\partial\bar{B}_{22}}{\partial\eta}\frac{\partial W}{\partial\eta}\frac{\partial^2 W}{\partial\eta^2}\end{array}\right)\end{array}\right)\\
&+\bar{B}_{11}\left(\left(\frac{\partial^2 W}{\partial\zeta^2}\right)^2+\frac{\partial W}{\partial\zeta}\frac{\partial^3 W}{\partial\zeta^3}\right)+\frac{1}{2}\frac{\partial^2\bar{B}_{11}}{\partial\zeta^2}\left(\frac{\partial W}{\partial\zeta}\right)^2+2\frac{\partial\bar{B}_{11}}{\partial\zeta}\frac{\partial W}{\partial\zeta}\frac{\partial^2 W}{\partial\zeta^2}\\
&+\bar{B}_{12}\beta^2\left(\frac{\partial W}{\partial\eta}\frac{\partial^3 W}{\partial\zeta^2\partial\eta}+\frac{\partial W}{\partial\zeta}\frac{\partial^3 W}{\partial\eta^2\partial\zeta}\right)+2\bar{B}_{12}\beta^2\left(\frac{\partial^2 W}{\partial\zeta\partial\eta}\right)^2\\
&+\frac{\beta^2}{2}\frac{\partial^2\bar{B}_{12}}{\partial\zeta^2}\left(\frac{\partial W}{\partial\eta}\right)^2+2\beta^2\frac{\partial\bar{B}_{12}}{\partial\zeta}\frac{\partial W}{\partial\eta}\frac{\partial^2 W}{\partial\zeta\partial\eta}\\
&+\frac{\beta^2}{2}\frac{\partial^2\bar{B}_{12}}{\partial\eta^2}\left(\frac{\partial W}{\partial\zeta}\right)^2+2\beta^2\frac{\partial\bar{B}_{12}}{\partial\eta}\frac{\partial W}{\partial\eta}\frac{\partial^2 W}{\partial\zeta\partial\eta}\\
&+2\beta^2\bar{B}_{66}\left(\frac{\partial^2 W}{\partial\zeta^2}\frac{\partial^2 W}{\partial\eta^2}+\left(\frac{\partial^2 W}{\partial\zeta\partial\eta}\right)^2+\left(\begin{array}{l}\frac{\partial W}{\partial\eta}\frac{\partial^3 W}{\partial\zeta^2\partial\eta}\\+\frac{\partial W}{\partial\zeta}\frac{\partial^3 W}{\partial\eta^2\partial\zeta}\end{array}\right)\right)\\
&+2\beta^2\left(\begin{array}{l}\frac{\partial^2\bar{B}_{66}}{\partial\zeta\partial\eta}\frac{\partial W}{\partial\zeta}\frac{\partial W}{\partial\eta}+\frac{\partial\bar{B}_{66}}{\partial\zeta}\left(\begin{array}{l}\frac{\partial W}{\partial\eta}\frac{\partial^2 W}{\partial\zeta\partial\eta}\\+\frac{\partial W}{\partial\zeta}\frac{\partial^2 W}{\partial\eta^2}\end{array}\right)+\frac{\partial\bar{B}_{66}}{\partial\eta}\left(\begin{array}{l}\frac{\partial^2 W}{\partial\zeta^2}\frac{\partial W}{\partial\eta}\\+\frac{\partial W}{\partial\zeta}\frac{\partial^2 W}{\partial\eta\partial\zeta}\end{array}\right)\end{array}\right)\\
&+\left(\bar{B}_{12}^*+2\bar{B}_{66}^*\right)\beta^2\left(\begin{array}{l}\frac{\partial^3 W}{\partial\zeta^2\partial\eta}\frac{\partial^2 W}{\partial\eta\partial\tau}+\frac{\partial^4 W}{\partial\zeta^2\partial\eta\partial\tau}\frac{\partial W}{\partial\eta}\\+\frac{\partial^3 W}{\partial\zeta\partial\eta^2}\frac{\partial^2 W}{\partial\zeta\partial\tau}+\frac{\partial W}{\partial\zeta}\frac{\partial^4 W}{\partial\zeta\partial\eta^2\partial\tau}\end{array}\right)\\
&+\bar{B}_{22}^*\beta^4\left(\frac{\partial^3 W}{\partial\eta^3}\frac{\partial^2 W}{\partial\eta\partial\tau}+2\frac{\partial^2 W}{\partial\eta^2}\frac{\partial^3 W}{\partial\eta^2\partial\tau}+\frac{\partial W}{\partial\eta}\frac{\partial^4 W}{\partial\eta^3\partial\tau}\right)+K_{nl}W^3+\bar{I}_0\frac{\partial^2 W}{\partial\tau^2}\\
&+2\bar{B}_{66}^*\beta^2\left(\frac{\partial^3 W}{\partial\zeta^2\partial\tau}\frac{\partial^2 W}{\partial\eta^2}+\frac{\partial^2 W}{\partial\zeta^2}\frac{\partial^3 W}{\partial\eta^2\partial\tau}\right)+K_l W-K_s\left(\frac{\partial^2 W}{\partial\zeta^2}+\beta^2\frac{\partial^2 W}{\partial\eta^2}\right)\\
&+\beta^2\left(\frac{\partial^2 W}{\partial\zeta^2}\frac{\partial^2\Theta}{\partial\eta^2}-2\frac{\partial^2 W}{\partial\zeta\partial\eta}\frac{\partial^2\Theta}{\partial\zeta\partial\eta}+\frac{\partial^2 W}{\partial\eta^2}\frac{\partial^2\Theta}{\partial\zeta^2}\right)-\gamma\left(\frac{\partial^4 W}{\partial\zeta^2\partial\tau^2}+\beta^2\frac{\partial^4 W}{\partial\eta^2\partial\tau^2}\right)\\
&-\chi^2\beta^2\left(\frac{\partial^4 W}{\partial\zeta^4}\frac{\partial^2\Theta}{\partial\eta^2}+2\frac{\partial^3 W}{\partial\zeta^3}\frac{\partial^3\Theta}{\partial\zeta\partial\eta^2}+\frac{\partial^2 W}{\partial\zeta^2}\frac{\partial^4\Theta}{\partial W^2\partial\eta^2}-4\frac{\partial^3 W}{\partial\zeta^2\partial\eta}\frac{\partial^3\Theta}{\partial\zeta^2\partial\eta}\right.\\
&\left.-2\frac{\partial^2 W}{\partial\zeta\partial\eta}\frac{\partial^4\Theta}{\partial\zeta^3\partial\eta}-2\frac{\partial^4 W}{\partial\zeta^3\partial\eta}\frac{\partial^2\Theta}{\partial\zeta\partial\eta}+\frac{\partial^2 W}{\partial\eta^2}\frac{\partial^4\Theta}{\partial\zeta^4}\right.\\
&\left.+\frac{\partial^4 W}{\partial\zeta^2\partial\eta^2}\frac{\partial^4\Theta}{\partial\zeta^4}+\beta^2\left(2\frac{\partial^3 W}{\partial\eta\partial\zeta^2}\frac{\partial^3\Theta}{\partial\eta^3}\right.\right.\\
&+2\frac{\partial^3 W}{\partial\eta^3}\frac{\partial^3\Theta}{\partial\zeta^2\partial\eta}+\frac{\partial^4 W}{\partial\eta^4}\frac{\partial^2\Theta}{\partial\zeta^2}+\frac{\partial^4 W}{\partial\zeta^2\partial\eta^2}\frac{\partial^2\Theta}{\partial\eta^2}-2\frac{\partial^2 W}{\partial\zeta\partial\eta}\frac{\partial^4\Theta}{\partial\zeta\partial\eta^3}\\
&-4\frac{\partial^3 W}{\partial\zeta\partial\eta^2}\frac{\partial^3\Theta}{\partial\zeta\partial\eta^2}+\frac{\partial^2 W}{\partial\zeta^2}\frac{\partial^4\Theta}{\partial\eta^4}+2\frac{\partial^3 W}{\partial\zeta^2\partial\eta}\frac{\partial^3\Theta}{\partial\eta^3}\\
&\left.\left.-2\frac{\partial^4 W}{\partial\zeta\partial\eta^3}\frac{\partial^2\Theta}{\partial\zeta\partial\eta}+\frac{\partial^2 W}{\partial\eta^2}\frac{\partial^4\Theta}{\partial\zeta^2\partial\eta^2}\right)\right)\\
&-\chi^2\left(K_l\left(\begin{array}{l}\frac{\partial^2 W}{\partial\zeta^2}\\+\beta^2\frac{\partial^2 W}{\partial\eta^2}\end{array}\right)-K_s\left(\begin{array}{l}\frac{\partial^4 W}{\partial\zeta^4}+2\beta^2\frac{\partial^4 W}{\partial\zeta^2\partial\eta^2}\\+\beta^4\frac{\partial^4 W}{\partial\eta^4}\end{array}\right)+6K_{nl}W\left(\frac{\partial W}{\partial\zeta}\right)^2\right.\\
&\left.+6K_{nl}W\beta^2\left(\frac{\partial W}{\partial\eta}\right)^2+3K_{nl}W^2\frac{\partial^2 W}{\partial\zeta^2}+3\beta^2K_{nl}W^2\frac{\partial^2 W}{\partial\eta^2}-\left(\begin{array}{l}\frac{\partial^4 W}{\partial\zeta^2\partial\tau^2}\\+\beta^2\frac{\partial^4 W}{\partial\eta^2\partial\tau^2}\end{array}\right)\right.\\
&\left.-\left(\frac{\partial^2\bar{I}_0}{\partial\zeta^2}\frac{\partial^2 W}{\partial\tau^2}+2\frac{\partial\bar{I}_0}{\partial\zeta}\frac{\partial^3 W}{\partial\zeta\partial\tau^2}+2\beta^2\frac{\partial\bar{I}_0}{\partial\eta}\frac{\partial^3 W}{\partial\eta\partial\tau^2}+\beta^2\frac{\partial^2\bar{I}_0}{\partial\eta^2}\frac{\partial^2 W}{\partial\tau^2}\right)\right.\\
&\left.+\left(\begin{array}{l}2\frac{\partial\bar{I}_2}{\partial\zeta}\left(\frac{\partial^5 W}{\partial\zeta^3\partial\tau^2}+\beta^2\frac{\partial^3 W}{\partial\zeta\partial\eta^2\partial\tau^2}\right)+\beta^2\frac{\partial^2\bar{I}_2}{\partial\eta^2}\left(\begin{array}{l}\frac{\partial^4 W}{\partial\zeta^2\partial\tau^2}\\+\beta^2\frac{\partial^4 W}{\partial\eta^2\partial\tau^2}\end{array}\right)\\+2\beta^2\frac{\partial\bar{I}_2}{\partial\eta}\left(\begin{array}{l}\frac{\partial^5 W}{\partial\zeta^2\partial\eta\partial\tau^2}\\+\beta^2\frac{\partial^5 W}{\partial\eta^3\partial\tau^2}\end{array}\right)+\beta^2\frac{\partial^2\bar{I}_2}{\partial\zeta^2}\frac{\partial^6 W}{\partial\eta^2\partial\tau^2}+\frac{\partial^2\bar{I}_2}{\partial\zeta^2}\frac{\partial^4 W}{\partial\zeta^2\partial\tau^2}\end{array}\right)\right.\\
&\left.+\bar{I}_2\left(\frac{\partial^6 W}{\partial\zeta^4\partial\tau^2}+\beta^2\frac{\partial^6 W}{\partial\zeta^2\partial\eta^2\partial\tau^2}+\beta^4\frac{\partial^6 W}{\partial\eta^4\partial\tau^2}\right)\right)=0
\end{aligned}
\tag{21}
$$

$$
\begin{aligned}
&\left(1-\chi\left(\frac{\partial^2}{\partial\zeta^2}+\beta^2\frac{\partial^2}{\partial\eta^2}\right)\right)\left[\begin{array}{l}\beta^4A_{11}^*\frac{\partial^4\Theta}{\partial\eta^4}+A_{22}^*\frac{\partial^4\Theta}{\partial\zeta^4}\\+\left(2A_{12}^*+A_{66}^*\right)\beta^2\frac{\partial^4\Theta}{\partial\zeta^2\partial\eta^2}\end{array}\right]\\
&=\beta^2\left(\left(\frac{\partial^2 W}{\partial\zeta\partial\eta}\right)^2-\frac{\partial^2 W}{\partial\zeta^2}\frac{\partial^2 W}{\partial\eta^2}\right)+\hat{\alpha}\beta^2\left(\begin{array}{l}\frac{\partial^2 W}{\partial\zeta\partial\eta}\frac{\partial^3 W}{\partial\zeta\partial\eta\partial\tau}\\-\frac{\partial^2 W}{\partial\zeta^2}\frac{\partial^3 W}{\partial\eta^2\partial\tau}-\frac{\partial^2 W}{\partial\eta^2}\frac{\partial^3 W}{\partial\zeta^2\partial\tau}\end{array}\right)
\end{aligned}
\tag{22}
$$

In a similar way, the boundary conditions for the simply supported case can be expressed as

$$
\begin{aligned}
&\eta=0,1: W=0,\ M_{\eta\eta}=0,\frac{\partial^2\bar{\Theta}}{\partial\zeta\partial\eta}=0,\ \bar{P}_y=\int_0^1\frac{\partial^2\bar{\Theta}}{\partial\zeta^2}d\zeta=0\\
&\zeta=0,1:\ W=0,\ M_{\zeta\zeta}=0,\frac{\partial^2\bar{\Theta}}{\partial\zeta\partial\eta}=0,\ \bar{P}_x=\int_0^1\frac{\partial^2\bar{\Theta}}{\partial\eta^2}d\eta=0
\end{aligned}
\tag{23}
$$

By considering the simply support boundary conditions, which are presented in Eq. (23), the transverse deflection can be assumed as

$$
W(\zeta,\eta,\tau)=q(\tau)\sin(\pi\zeta)\sin(\pi\eta),
\tag{24}
$$

Also, by inserting Eq. (24) into Eq. (22), the Airy's function can be obtained as

$$\bar{\Theta}=c_1(\tau)\cos(2\pi\zeta)+c_2(\tau)\cos(2\pi\eta)+c_3(\tau)\frac{x^2}{2}+c_4(\tau)\frac{y^2}{2} \tag{25}$$

The unknown coefficients in the above equations are described as

$$\begin{aligned}
&c_1(\tau)=\frac{\beta^2 q(\tau)}{\Gamma_1}\left(q(\tau)+2\hat{\alpha}\frac{dq(\tau)}{d\tau}\right),\\
&c_2(\tau)=\frac{q(\tau)}{\Gamma_2}\left(q(\tau)+2\hat{\alpha}\frac{dq(\tau)}{d\tau}\right)\\
&\Gamma_1=16A_{22}^*\left(\left(2+8\pi^2\chi_{ce}^2\right)X(\zeta)Y(\eta)+\chi_{ce}^2\left(\begin{matrix}\beta^2X(\zeta)\frac{d^2Y(\eta)}{d\eta^2}\\+\frac{d^2X(\zeta)}{d\zeta^2}Y(\eta)\end{matrix}\right)\right)\\
&\Gamma_2=16A_{11}^*\beta^2\left(\left(2+8\pi^2\chi_{ce}^2\right)X(\zeta)Y(\eta)+\chi_{ce}^2\left(\begin{matrix}\beta^2X(\zeta)\frac{d^2Y(\eta)}{d\eta^2}\\+\frac{d^2X(\zeta)}{d\zeta^2}Y(\eta)\end{matrix}\right)\right)
\end{aligned} \tag{26}$$

Also, by using the boundary conditions, which are described in Eq. (23), one can easily obtain

$$c_3(\tau)=0,\ c_4(\tau)=0 \tag{27}$$

The coefficients of the Airy's function, which are presented in Eq. (26) and Eq. (27), are shown that the small scale parameters appear them. Here, Eq. (24) and Eq. (25) insert in Eq. (21) and the Bubonov-Galerkin method is used to discrete the nonlinear partial differential equation to a nonlinear ordinary differential equation. To this end, one can easily obtain

$$\int_0^1\int_0^1 \Upsilon\left[\Xi(\zeta,\eta)\right]\Xi(\zeta,\eta)d\zeta d\eta=0 \tag{28}$$

In the Bubonov-Galerkin method, which is described in the previous equation, the notation $\Xi(\zeta,\eta)$ is presented the base function. By considering simply supported boundary conditions, the base function for can show as

$$\Xi(\zeta,\eta)=\sin(\pi\zeta)\sin(\pi\eta) \tag{29}$$

Further, the operator Υ can be obtained as Eq. (22). By using some mathematical simplifications, Eq. (28) can be rewritten as

$$\begin{aligned}
&\frac{d^2q(\tau)}{d\tau^2}+\alpha_1q(\tau)+\alpha_2\left(q(\tau)\right)^2+\alpha_3\left(q(\tau)\right)^3+\alpha_4q(\tau)\frac{dq(\tau)}{d\tau}\\
&+\alpha_5\left(q(\tau)\right)^2\frac{dq(\tau)}{d\tau}+\alpha_6\frac{dq(\tau)}{d\tau}=\bar{F}\cos(\Omega\tau)
\end{aligned} \tag{30}$$

The coefficients $\alpha_i\left(i=1,...,6\right)$ in the above equation are obtained from Eq. (28). Based on the physical neutral surface concept, the physical neutral surface of FGM beam is given as (Ebrahimi and Salari 2015)

$$z_0=\frac{\int_{-(h_c/2+h_l)}^{-(h_c/2)}E_l\,z\,dz+\int_{-h_c/2}^{h_c/2}E_c(z)\,z\,dz+\int_{(h_c/2)}^{(h_c/2+h_l)}E_l\,z\,dz}{\int_{-(h_c/2+h_l)}^{-(h_c/2)}E_l\,dz+\int_{-h_c/2}^{h_c/2}E_c(z)\,dz+\int_{(h_c/2)}^{(h_c/2+h_l)}E_l\,dz} \tag{31}$$

It can be seen that the physical neutral surface and the geometric middle surface are the same in a homogeneous isotropic nanoplate. The coefficients α_2 and α_4 will be zero as the new reference surface position is utilized.

By this definition, the coefficients $a_i, b_i\left(i=0,1,2\right)$ in Eq. (17), Eqs. (23)-(25) and Eqs. (28)-(29) are described as

$$\begin{aligned}
&a_0=-\left(\frac{h_c-2z_0}{2}\right),\ a_1=-\left(\frac{h_c-2z_0}{2}\right),a_2=-\left(\frac{h_c-2z_0}{2}+h_l\right),\\
&b_0=\frac{h_c+2z_0}{2}\quad,\ b_1=\left(\frac{h_c+2z_0}{2}\right)\ ,b_2=\left(\frac{h_c+2z_0}{2}+h_l\right),
\end{aligned} \tag{32}$$

By applying the new reference surface in the calculation of the constants, Eq. (30) is changed as

$$\begin{aligned}
&\frac{d^2q(\tau)}{d\tau^2}+\omega_n^2q(\tau)+\alpha_a\left(q(\tau)\right)^3+\alpha_b\left(q(\tau)\right)^2\frac{dq(\tau)}{d\tau}\\
&+\alpha_c\frac{dq(\tau)}{d\tau}=F\cos(\Omega\tau)
\end{aligned} \tag{33}$$

In the previous equation, in order to simplify, the constants α_1, α_3, α_5 and α_6 in Eq. (30) are replaced by ω_n^2, α_a, α_b and α_c respectively.

3. Solution method

In this section, the solution method of the nonlinear ordinary differential equation, which is represented in Eq. (33), is explained. To solve the nonlinear ordinary differential equation, the multiple scales method is applied. According to the multiple scales method, the solution of Eq. (33) is assumed to be as

$$q(\tau,\varepsilon)=q_0(T_0,T_1)+\varepsilon q_1(T_0,T_1) \tag{34}$$

In this equation, the letters τ and $\varepsilon\tau$ are determined by T_0 and T_1. Moreover, the first and second order derivatives are defined as

$$\begin{aligned}
&\frac{d}{d\tau}=D_0+\varepsilon D_1+\varepsilon^2D_2\\
&\frac{d^2}{d\tau^2}=D_0^2+\varepsilon 2D_0D_1+\varepsilon^2\left(D_1^2+2D_0D_2+....\right)
\end{aligned} \tag{34}$$

The symbol D_n is defined the $d/d\tau^n$. By inserting Eq. (34) and Eq. (35) into Eq. (33), gives

$$\begin{aligned}
&\left(D_0^2+\varepsilon 2D_0D_1+\varepsilon^2\left(D_1^2+2D_0D_2\right)\right)\left(\begin{matrix}q_0(T_0,T_1)+\varepsilon q_1(T_0,T_1)\\+\varepsilon^2q_2(T_0,T_1)+O\left(\varepsilon^3\right)\end{matrix}\right)\\
&+\omega_n^2\left(q_0(T_0,T_1)+\varepsilon q_1(T_0,T_1)+\varepsilon^2q_2(T_0,T_1)+O\left(\varepsilon^3\right)\right)\\
&+\varepsilon\alpha_a\left(q_0(T_0,T_1)+\varepsilon q_1(T_0,T_1)+\varepsilon^2q_2(T_0,T_1)+O\left(\varepsilon^3\right)\right)^3\\
&\quad+\varepsilon\alpha_b\left(\begin{matrix}q_0(T_0,T_1)+\varepsilon q_1(T_0,T_1)\\+\varepsilon^2q_2(T_0,T_1)+O\left(\varepsilon^3\right)\end{matrix}\right)^2\left(\begin{matrix}D_0+\varepsilon D_1\\+\varepsilon^2D_2+O\left(\varepsilon^3\right)\end{matrix}\right)\\
&\quad\left(\begin{matrix}q_0(T_0,T_1)+\varepsilon q_1(T_0,T_1)\\+\varepsilon^2q_2(T_0,T_1)+O\left(\varepsilon^3\right)\end{matrix}\right)\\
&+\varepsilon\alpha_c\left(D_0+\varepsilon D_1+\varepsilon^2D_2\right)\left(\begin{matrix}q_0(T_0,T_1)+\varepsilon q_1(T_0,T_1)\\+\varepsilon^2q_2(T_0,T_1)+O\left(\varepsilon^3\right)\end{matrix}\right)=\varepsilon F\cos(\Omega\tau)
\end{aligned} \tag{36}$$

By separating the like power of small dimensionless

parameters, Eq. (36) can be separated as

$$\begin{aligned}
&\varepsilon^0:\ D_0^2 q_0+\omega_n^2 q_0=0\\
&\varepsilon^1:\ D_0^2 q_1+\omega_n^2 q_1=-2D_0D_1q_0-\alpha_a q_0^3-\left(\alpha_b q_0^2+\alpha_c\right)D_0q_0+F\cos\left(\Omega\tau\right)\\
&=-2i\omega_n D_1 A e^{i\omega_n T_0}-\alpha_c i\omega_n A e^{i\omega_n T_0}-3\alpha_a A^2\bar{A}e^{i\omega_n T_0}-\alpha_b i\omega_n A^2\bar{A}e^{i\omega_n T_0}\\
&-\alpha_a A^3 e^{3i\omega_n T_0}-\alpha_b i\omega_n A^3 e^{3i\omega_n T_0}+\frac{F}{2}\cos\left(\Omega\tau\right)+CC
\end{aligned}\tag{37}$$

In the previous equation, the phrase CC refers to the conjugate terms. The non-resonance, primary and secondary resonance cases are studied in the next section.

3.1 The non-resonance case

In this section, it is assumed that the excitation frequency is far from the linear natural frequency. According to this assumption, the secular terms of Eq. (37) should be eliminated as

$$-2i\omega_n D_1 A e^{i\omega_n T_0}-\alpha_c i\omega_n A e^{i\omega_n T_0}-3\alpha_a A^2\bar{A}e^{i\omega_n T_0}-\alpha_b i\omega_n A^2\bar{A}e^{i\omega_n T_0}\tag{38}$$

In the previous equation, the parameters A is considered as a complex number as the following form

$$A\left(T_1\right)=\frac{1}{2}a\left(T_1\right)e^{i\beta\left(T_1\right)}\tag{39}$$

As Eq. (39) is inserted in Eq. (38) and the real and imaginary part of Eq. (38) are separated as

$$\text{Im}:\qquad \frac{da}{dT_1}=-\frac{\alpha_b}{8}a^3-\frac{4}{8}\alpha_c a\tag{40}$$

$$\text{Re}:\qquad \frac{d\beta}{dT_1}=\frac{3}{8\omega_n}\alpha_a a^2\tag{41}$$

To solve Eq. (40) and Eq. (41), the ordinary differential equation techniques are utilized. Thus, the solutions of Eq. (40) and Eq. (41) can calculate as

$$a\left(T_1\right)=\left(\frac{\frac{4\alpha_c}{\alpha_b}e^{\left(-\alpha_c T_1\right)}}{\left(1-e^{\left(-\alpha_c T_1\right)}\right)+4\frac{\alpha_c}{\alpha_b A_0^2}}\right)^{\frac{1}{2}}\tag{42}$$

$$\beta\left(T_1\right)=\frac{3\alpha_a}{2\alpha_b\omega_n}\ln\left(1-e^{\left(-\alpha_c T_1\right)}+4\frac{\alpha_c}{\alpha_b A_0^2}\right)+\beta_0\tag{43}$$

In the previous relations, the parameters A_0 and β_0 explain the initial amplitude and initial phase angle, respectively. One can obtain the solution of Eq. (37), as the secular terms are eliminated. To this end, the time functions $q_0\left(T_0,T_1\right)$ and $q_1\left(T_0,T_1\right)$ are obtained. It is important to note that the parameters T_0 and T_1 in the previous section should be replaced by τ and $\varepsilon\tau$, respectively. Thus, the time function $q(\tau)$ can be obtained as

$$\begin{aligned}
q\left(\tau\right)&=\left(\frac{\frac{4\alpha_c}{\alpha_b}e^{\left(-\alpha_c\varepsilon\tau\right)}}{\left(1-e^{\left(-\alpha_c\varepsilon\tau\right)}\right)+4\frac{\alpha_c}{\alpha_b A_0^2}}\right)^{\frac{1}{2}}\\
&\cos\left(\omega_n\tau+\frac{3\alpha_a}{2\alpha_b\omega_n}\ln\left(1-e^{\left(-\alpha_c\varepsilon\tau\right)}+4\frac{\alpha_c}{\alpha_b A_0^2}\right)+\beta_0\right)\\
&+\frac{\varepsilon}{32\omega_n^2}\left(\frac{\frac{4\alpha_c}{\alpha_b}e^{\left(-\alpha_c\varepsilon\tau\right)}}{\left(1-e^{\left(-\alpha_c\varepsilon\tau\right)}\right)+4\frac{\alpha_c}{\alpha_b A_0^2}}\right)^{\frac{3}{2}}\\
&\left\{\alpha_a\cos\left(3\omega_n\tau+\frac{9\alpha_a}{2\alpha_b\omega_n}\ln\left(1-e^{\left(-\alpha_c\varepsilon\tau\right)}+4\frac{\alpha_c}{\alpha_b A_0^2}\right)+\beta_0\right)\right.\\
&\left.-\alpha_b\sin\left(3\omega_n\tau_0+\frac{9\alpha_a}{2\alpha_b\omega_n}\ln\left(1-e^{\left(-\alpha_c\varepsilon\tau\right)}+4\frac{\alpha_c}{\alpha_b A_0^2}\right)+\beta_0\right)\right\}\\
&+\frac{F}{2\left(\omega_n^2-\Omega^2\right)}\cos\left(\Omega\tau\right)
\end{aligned}\tag{44}$$

3.2 The primary resonance case

As the excitation frequency is near to the linear natural frequency, the primary resonance will happen. In this section, the frequency analysis of the sandwich nanoplate is studied in the primary resonance case. To this end, it is assumed that the excitation frequency is very near to the linear natural frequency of the sandwich nanoplate ($\Omega=\omega_n+\varepsilon\sigma$). The symbols σ and ε are the detuning and the small dimensionless parameters. To achieve the primary resonance case, the Eq. (33) is rewritten as

$$\begin{aligned}
&\ddot{q}(\tau)+\omega_n^2 q(\tau)+\varepsilon\left(\alpha_a q^3(\tau)+\alpha_b q^2(\tau)\dot{q}(\tau)+\alpha_c\dot{q}(\tau)\right)\\
&=\varepsilon F\cos(\Omega\tau)
\end{aligned}\tag{45}$$

In the similar way, the real and imaginary parts of the secular terms in the primary resonance case are obtained as

$$\text{Re}:\qquad \omega_n a\frac{d\beta}{dT_1}=\frac{3}{8}\alpha_a a^3-\frac{F}{2}\cos\left(\gamma\right)\tag{46}$$

$$\text{Im}:\qquad \omega_n\frac{da}{dT_1}=-\frac{\alpha_b}{8}a^3-\frac{4}{8}\alpha_c a-\frac{F}{2}\sin\left(\gamma\right)\tag{47}$$

It is assumed that the steady state is stablished $a'=\gamma'=0$. After some triangular simplification, Eq. (46) and Eq. (47) are changed as

$$\left(\frac{\alpha_b}{8}a^3+\frac{4}{8}\alpha_c a\right)^2+\left(\sigma a-\frac{3\alpha_a}{8\omega_n}a^3\right)^2=\frac{F^2}{4\omega_n^2}\tag{48}$$

The detuning-amplitude relation in the steady state can be obtained from Eq. (48) as

$$\sigma=\frac{3\alpha_a a^2}{8\omega_n}\pm\sqrt{\left(\frac{F}{2a\omega_n}\right)^2-\left(\frac{\alpha_c}{2}+\frac{\alpha_b a^2}{8}\right)^2} \tag{49}$$

3.3 The secondary resonance case

In this section, the secondary resonance case is studied. The super harmonic and subharmonic resonance are subsection of the secondary resonance case. To investigate the secondary resonance case, Eq. (33) is rewritten as

$$\begin{aligned}&\ddot{q}(\tau)+\omega_n^2 q(\tau)+\varepsilon\left(\alpha_a q^3(\tau)+\alpha_b q^2(\tau)\dot{q}(\tau)+\alpha_c\dot{q}(\tau)\right)\\&=\frac{F}{2}\left(e^{i\Omega\tau}+e^{-i\Omega\tau}\right)\end{aligned} \tag{50}$$

Here, the cosine term is rewritten as the exponential term. Eq. (34) and the Eq. (35) are inserted in the Eq. (50) and the terms with same power small dimensionless parameter are collected together as

$$\varepsilon^0:\quad D_0^2 q_0+\omega_n^2 q_0=\frac{F}{2}\left(e^{i\Omega T_0}+e^{-i\Omega T_0}\right) \tag{51a,b}$$

$$\varepsilon^1:\quad D_0^2 q_1+\omega_n^2 q_1=-2D_0D_1q_0-\alpha_a q_0^3-\alpha_b q_0^2 D_0 q_0-\alpha_c D_0 q_0$$

The standard solution of the ordinary differential equation is as

$$q_0=A\,\mathrm{e}^{i\omega_n T_0}+\bar{A}\,\mathrm{e}^{-i\omega_n T_0}+\Lambda\left(e^{i\Omega T_0}+e^{-i\Omega T_0}\right),\Lambda=\frac{F}{2\left(\omega_n^2-\Omega^2\right)} \tag{52}$$

Eq. (52) is inserted into Eq. (51b) as

$$\begin{aligned}&D_0^2 q_1+\omega_n^2 q_1=-2i\omega_n D_1 A e^{i\omega_n T_0}+2i\omega_n D_1\bar{A}e^{-i\omega_n T_0}\\&-\alpha_a\left(A\,\mathrm{e}^{i\omega_n T_0}+\bar{A}\,\mathrm{e}^{-i\omega_n T_0}+\Lambda\left(e^{i\Omega T_0}+e^{-i\Omega T_0}\right)\right)^3\\&-\alpha_b\left(i\omega_n A e^{i\omega_n T_0}-i\omega_n A e^{-i\omega_n T_0}+i\Lambda\left(e^{i\Omega T_0}-e^{-i\Omega T_0}\right)\right)\left(\begin{matrix}A\,\mathrm{e}^{i\omega_n T_0}+A\,\mathrm{e}^{-i\omega_n T_0}\\+\Lambda\left(e^{i\Omega T_0}+e^{-i\Omega T_0}\right)\end{matrix}\right)^2\\&-\alpha_c\left(i\omega_n A e^{i\omega_n T_0}-i\omega_n A e^{-i\omega_n T_0}+i\Lambda\left(e^{i\Omega T_0}-e^{-i\Omega T_0}\right)\right)\end{aligned} \tag{53}$$

The expressions exponents must be calculated and then some mathematical simplifications should be done in Eq. (53). Two different resonance cases are detected in Eq. (53) that each of them is investigated separately.

3.3.1 The super harmonic resonance case

The super harmonic resonance cases of the Eq. (53) are studied in this section. The super harmonic resonance happens when the non-dimensional excitation frequency is near close to the one third of the natural frequency ($3\Omega=\omega_n+\varepsilon\sigma$). The secular terms in the real and imaginary parts are obtained as

$$\begin{aligned}&\mathrm{Re}:\ \frac{1}{2}\alpha_c a\omega_n+\omega_n\frac{da}{dT_1}+\frac{1}{8}\alpha_b a^3\omega_n+\alpha_b a\omega_n\Lambda^2\\&\quad+\Lambda^3\alpha_a\sin\gamma+\Lambda^3\alpha_b\Omega\cos\gamma=0\\&\mathrm{Im}:\ \frac{3}{8}\alpha_a a^3+3\alpha_a a\Lambda^2+\omega_n a\frac{d\gamma}{dT_1}\\&\quad-\omega_n a\sigma+\alpha_a\Lambda^3\cos\gamma-\alpha_b\sin\gamma=0\end{aligned} \tag{54}$$

The symbol γ is defined $\gamma=\sigma T_1-\beta(T_1)$. By considering the steady state condition and some simplification roles, the detuning-amplitude relation for this case is obtained as

$$\begin{aligned}\sigma&=\frac{3}{8\omega_n}\alpha_a a^2+\frac{3\alpha_a}{\omega_n}\Lambda^2\\&+\left(\left(\left(\frac{\alpha_a\Lambda^3}{\omega_n a}\right)^2+\left(\frac{\alpha_b\Omega\Lambda^3}{\omega_n a}\right)^2\right)-\left(\alpha_b\Lambda^2+\frac{1}{8}\alpha_b a^2+\frac{1}{2}\alpha_c\right)^2\right)^{\frac{1}{2}}\end{aligned} \tag{55}$$

3.3.2 The sub harmonic resonance case

The sub harmonic resonance case happens when the non-dimensional excitation frequency is near to triple of the natural frequency ($\Omega=3\omega_n+\varepsilon\sigma$). Similar to the previous section, the secular terms are divided to the real and the imaginary parts. After some mathematical simplification the frequency-amplitude relation for this case is obtained as

$$\begin{aligned}&\alpha_a^2\omega_n^2\left(\frac{9\alpha_a a^2}{24\omega_n}+\frac{3\alpha_a}{\omega_n}\Lambda^2+\frac{\alpha_b^2\Omega a^2}{8\alpha_a}+\frac{\alpha_b^2\Omega\Lambda^2 a^2}{\alpha_a}-\frac{\sigma}{3}\right)^2\\&+\alpha_b^2\Omega^2\omega_n^2\left(\frac{\alpha_a a^2}{8\Omega}+\frac{\alpha_a\Lambda^2}{\Omega}-\frac{3\alpha_a a^2}{8\omega_n}-\frac{3\alpha_a\Lambda^2}{\omega_n}+\frac{\sigma}{3}\right)^2\\&=\left(\left(\alpha_a^2+\alpha_b^2\Omega^2\right)\Lambda^3\right)^2\end{aligned} \tag{56}$$

4. Results and discussion

In this section, the numerical results of the vibration analysis of the composite nanoplate are presented. The first, the validation is presented between the numerical results and the reported results in the literature. Also, the presented results are compared with the Runge-Kutta results. Finally, the force vibration of the composite nanoplate is studied and the numerical results of the primary and secondary resonance cases are presented. The material properties of the FG core are taken from Refs (Ebrahimi and Jafari 2018). The physical properties of the system are assumed as the stated in this section, unlike there is another thing stated. The length of the composite nanoplate and the aspect ratio (the ratio of the length to width) are considered 50 nm and 1, respectively. The Winkler elastic, the shear elastic and the nonlinear elastic constants are assumed 100, 5 and 10, respectively.

4.1 Validation

To ensure about the numerical results, the present results are compared with the reported results in the literature (Ebrahimi and Hosseini 2016). To done this validate, it is assumed that the effect of the FG core is neglected. Fig. 3 shows the comparison between the numerical results and the reported results (Ebrahimi and Hosseini 2016). These results are presented for two different aspect ratios. It is completely obvious that the presented results are in good agreement with the reported results in the literature (Ebrahimi and Hosseini 2016).

In order to more validate, the numerical results are compared with the results which are obtained by the Runge-Kutta method. Fig. 4 illustrates the time history for the composite nanoplate versus the non-dimensional time. To plot this figure, it is assumed that the composite nanoplate is fabricated by the FG core and lipid layers. One can easily see that the results of the multiple scale method are matched with the Runge-Kutta results.

4.2 Free vibration results

The time history of the composite nanoplate is shown in Fig. 5(a)-(d). The effects of the porosity distribution type and the aspect ratio (the ratio of the length to width of the composite nanoplate) on the time history of the composite nanoplate are studied. In Figs. 5(a)-(d), the effect of the lipid layer is considered and it is seen that the time history is damped over time. In Fig. 5(b) and Fig. 5(d), the aspect ratio is considered β=4 and in other figures this parameter is taken β=2. Fig. 5(c) and Fig. 5(d) are plotted by considering the X distribution type and the O distribution type is considered for other figures. These figures reveal this fact that the porosity distribution type and the aspect ratio have dramatic effect on the time history of the composite nanoplate. The time history is damped faster as the aspect ratio increases. Further, the time history is damped faster as the porosity distribution is X type. This is because that the porosity of the FG core in type X is more than type O. It is caused by that the stiffness of the system decreases and the vibration amplitude is damped faster. This means that the porosity distribution type has an important effect on the dynamical response of the composite nanoplate.

The phase diagram for the X and O porosity distribution type is shown in Fig. 6. Other parameters for two type distributions are same. It is shown that the equilibrium point is spiral sink at (0, 0) and the phase diagram is spiral in two types. This figure shows that the phase diagram in X distribution type is damped faster than that in the O distribution type. This phenomenon reveals this fact that the distribution type changes the damping of the system. Thus, the system with X distribution type has higher value of damping than the system with O distribution type.

The frequency ratio versus the amplitude of the nanoplate is shown in Fig. 7. This figure reveals that the difference between the numerical results in the X distribution type and the O distribution type increases as the amplitude of the nanoplate increases. The frequency ratio of the X distribution type is always more than that the O distribution type. Moreover, the frequency ratio decreases as the structural damping increases. The gap between the curves by different structural damping and same distribution type increases as the amplitude increases.

The nonlinear vibration frequency versus time is illustrated in Fig. 8. This figure is plotted for different elastic medium type. This figure displays that the nonlinear vibration frequency is decreased by passing the time. Moreover, the nonlinear vibration frequency in the nonlinear type of the elastic medium is more than that the linear elastic medium type. The nonlinear elastic type has

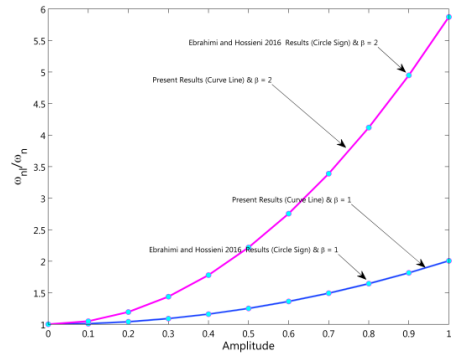

Fig. 3 Comparison between the present results and the reported results (Ebrahimi and Hosseini 2016)

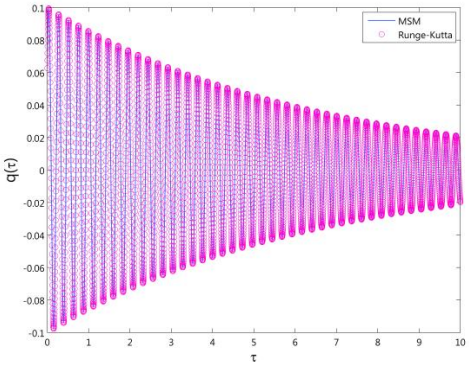

Fig. 4 Comparison between the results of the Multiple Scale Method (MSM) and the Runge-Kutta results

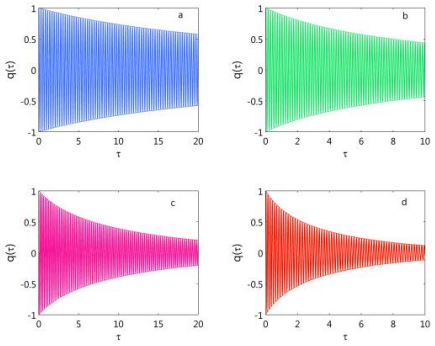

Fig. 5 Change of the time history for different aspect ratios and porosity distribution types. (a) O distribution type and β=2. (c) X distribution type and β=2. (d) X distribution type and β=4

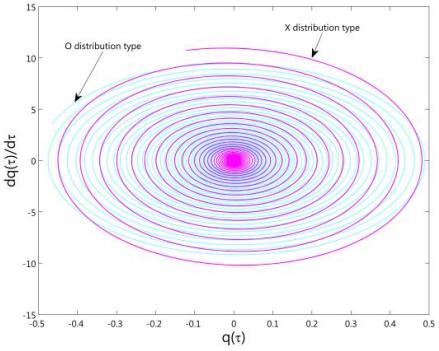

Fig. 6 Phase diagram for two different porosity distribution types

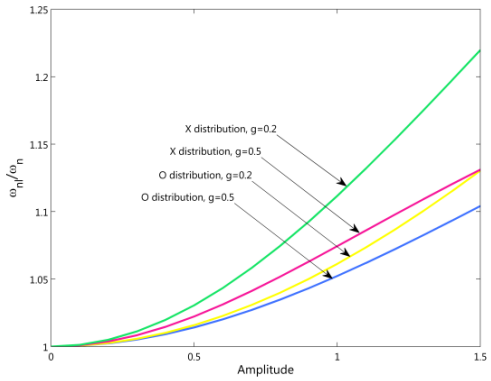

Fig. 7 Change of the frequency ratio respect amplitude for different porosity types and structural damping

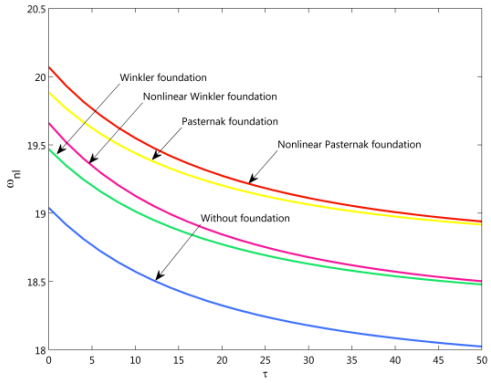

Fig. 8 Change of the nonlinear frequency versus time for different elastic foundation types

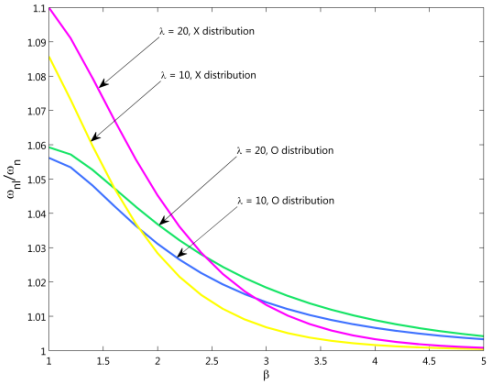

Fig. 9 Change of the frequency ratio versus aspect ratio for different porosity distribution types

significant effect in lower amount of time. By passing a time, the effect of the nonlinear elastic medium is vanished. This is because that the nonlinear part of the frequency decreases as exponential form and the nonlinear frequency intend to linear frequency through the time.

Fig. 9 is shown the effect of the aspect ratio and the ratio on the frequency ratio. The decreasing effect of the aspect ratio on the frequency ratio is shown clearly in this figure. The decay rate of the aspect ratio on the frequency ratio in the X distribution type is more than the O distribution type. Unlike the aspect ratio, the area ratio has increasing effect on the frequency ratio. Fig. 9 exhibits that the area ratio has

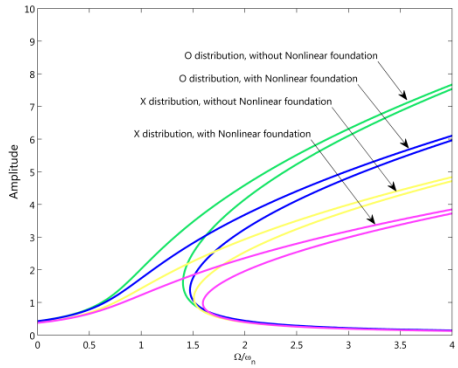

Fig. 10 Frequency-amplitude curves for different porosity distribution and elastic foundation types

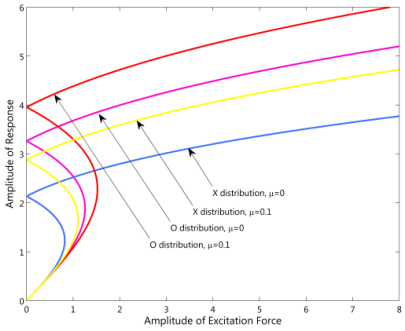

Fig. 11 Amplitude of response versus amplitude of excitation force for different porosity distribution types and nonlocal parameters

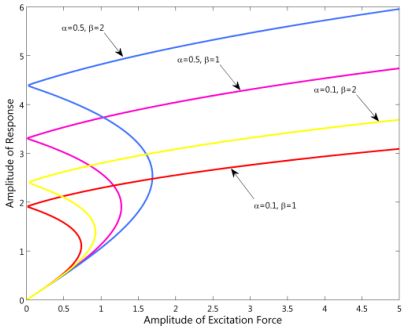

Fig. 12 Amplitude of response versus amplitude of excitation force for different porosity volume fractions and aspect ratio parameters

dramatic effect in the smaller aspect ratio.

5. Force vibration results

In this section, the numerical results of the nonlinear force vibration of the composite nanoplate are presented.

The amplitude-frequency curve is plotted in Fig. 10. In this figure, the influences of distribution types and the foundation are investigated. It is completely obvious that the nonlinearity of the system is more in the FG core with X distribution type rather than the O distribution type. This is because that the amplitude-frequency curves bend away to right side as the distribution type changes to X type. Moreover, the system shows a hardening behavior as the

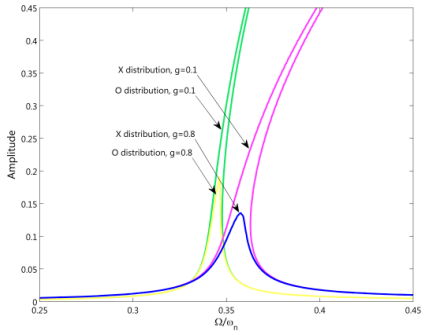

Fig. 13 Frequency-amplitude curves for different porosity distribution and structural damping parameters and super harmonic resonance case

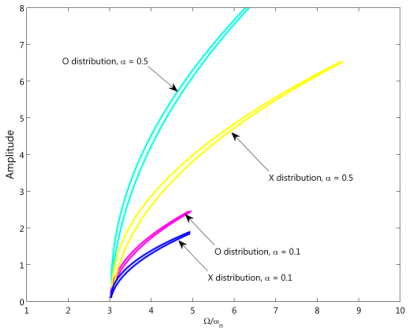

Fig. 14 Frequency-amplitude curves for different porosity distribution types and volume fraction porosity parameters

composite nanoplate is located on the foundation. This is because that the nonlinear part of the governing equation increases as the system is embedded on the foundation.

Fig. 11 is shown the vibration amplitude versus the amplitude of the excitation force. Two different distribution porosities are investigated in the local and nonlocal solution cases.

It is clear that the composite nanoplate in the local case shows more stiffness behavior than that the nonlocal case. Thus, the local solution with X distribution porosity type shows the most stiffness behavior in compare with other cases. This is because that the nonlocal parameter decreases the stiffness of the composite nanoplate.

The influences of the aspect ratio and the porosity volume fraction are investigated in Fig. 12. This figure is shown that the nonlinearity of the system is related to the aspect ratio and the porosity volume fraction. The aspect ratio and the porosity volume fraction have same effect on the nonlinearity of the system. Thus, the nonlinearity of the system decreases as the aspect ratio or the porosity volume fraction increases. These are obviously facts because the stiffness of the system decreases by creating the porosity in the core of system. Furthermore, the flexibility of the system increases as the aspect ratio increases and the shape of the nanoplate changes to nanobeam.

The super harmonic resonance case is shown in Fig. 13. In this figure, the influences of the damping structure and porosity volume fraction on the backbone curves are studied. It is obvious that the structural damping decreases the peak of the amplitude-frequency curves. Also, the influences of the porosity distribution types on the super harmonic resonance are distinguished. The system with X distribution type shows more stiffness than the system with the O distribution type.

The effects of the porosity distribution types and the porosity volume fraction on the subharmonic resonance case are investigated in Fig. 14. This figure confirms the obtained results in the previous figures. This figure shows that the effect of the porosity distribution type on the amplitude-frequency curves in the subharmonic resonance case and the super harmonic resonance case is similar. This figure reveals that the porosity volume fraction on the hardening of the system has decreasing effect in the subharmonic resonance case. It is obvious that the stiffness of the system decreases by creating the porosity in the FG core.

6. Conclusions

In this study, the nonlinear vibration analysis of the composite nanoplate is studied. It is assumed that the core of the composite nanoplate is fabricated by three directional functional graded. This is the first time that the nonlinear vibration composite nanoplate with three directional FG materials is investigated. The core of the nanoplate is covered by the lipid layers at top and bottom of it. The influences of two different porosity distribution types on the nonlinear vibration behavior are studied. The primary and the secondary resonance cases are considered. The following points are revealed by this study:

• The porosity distribution types change the stiffness of the system.

• The time effect on the time history of the system with X distribution porosity is more important in compare with the O distribution type.

• The frequency ratio is changed by the structural damping and the amplitude of the composite nanoplate.

• The nonlinear foundation increases the nonlinearity of the system.

• The aspect ratio and the porosity volume fraction decrease the hardening of the system.

References

Ajri, M. and Fakhrabadi, M.M.S. (2018), "Nonlinear free vibration of viscoelastic nanoplates based on modified couple stress theory", *J. Comput. Appl. Mech.*, **49**(1).

Ashofteh, A., Mashhadi, M.M. and Amadeh, A. (2018), "Effect of nano-structuration and compounding of YSZ APS TBCs with different thickness on coating performance in thermal shock conditions", *J. Comput. Appl. Mech.*, **49**(1), 18-26.

Belmahi, S., Zidour, M., Meradjah, M., Bensattalah, T. and Dihaj, A. (2018), "Analysis of boundary conditions effects on vibration of nanobeam in a polymeric matrix", *Struct. Eng. Mech.*, **67**(5), 517-525.

Bogdanski, D., Köller, M., Müller, D., Muhr, G., Bram, M., Buchkremer, H.P., Stöver, D., Choi, J. and Epple, M. (2002), "Easy assessment of the biocompatibility of Ni-Ti alloys by in vitro cell culture experiments on a functionally graded Ni-NiTi-Ti material", *Biomater.*, **23**(23), 4549-4555.

Ebrahimi, F. and Barati, M.R. (2016), "Dynamic modeling of a

thermo-piezo-electrically actuated nanosize beam subjected to a magnetic field", *Appl. Phys. A*, **122**(4), 451.
Ebrahimi, F. and Barati, M.R. (2017), "Buckling analysis of nonlocal third-order shear deformable functionally graded piezoelectric nanobeams embedded in elastic medium", *J. Brazil. Soc. Mech. Sci. Eng.*, **39**(3), 937-952.
Ebrahimi, F. and Barati, M.R. (2017), "Porosity-dependent vibration analysis of piezo-magnetically actuated heterogeneous nanobeams", *Mech. Syst. Sign. Proc.*, **93**, 445-459.
Ebrahimi, F. and Barati, M.R. (2017), "Small-scale effects on hygro-thermo-mechanical vibration of temperature-dependent nonhomogeneous nanoscale beams", *Mech. Adv. Mater. Struct.*, **24**(11), 924-936.
Ebrahimi, F. and Barati, M.R. (2017), "Through-the-length temperature distribution effects on thermal vibration analysis of nonlocal strain-gradient axially graded nanobeams subjected to nonuniform magnetic field", *J. Therm. Stress.*, **40**(5), 548-563.
Ebrahimi, F. and Barati, M.R. (2018), "A unified formulation for modeling of inhomogeneous nonlocal beams", *Struct. Eng. Mech.*, **66**(3), 369-377.
Ebrahimi, F. and Barati, M.R. (2018), "Vibration analysis of piezoelectrically actuated curved nanosize FG beams via a nonlocal strain-electric field gradient theory", *Mech. Adv. Mater. Struct.*, **25**(4), 350-359.
Ebrahimi, F. and Barati, M.R. (2018), "Vibration analysis of smart piezoelectrically actuated nanobeams subjected to magneto-electrical field in thermal environment", *J. Vibr. Contr.*, **24**(3), 549-564.
Ebrahimi, F., Barati, M.R. and Haghi, P. (2017), "Thermal effects on wave propagation characteristics of rotating strain gradient temperature-dependent functionally graded nanoscale beams", *J. Therm. Stress.*, **40**(5), 535-547.
Ebrahimi, F. and Dabbagh, A. (2017), "Nonlocal strain gradient based wave dispersion behavior of smart rotating magneto-electro-elastic nanoplates", *Mater. Res. Expr.*, **4**(2), 025003.
Ebrahimi, F. and Dabbagh, A. (2017), "On flexural wave propagation responses of smart FG magneto-electro-elastic nanoplates via nonlocal strain gradient theory", *Compos. Struct.*, **162**, 281-293.
Ebrahimi, F. and Farazmandnia, N. (2017), "Thermo-mechanical vibration analysis of sandwich beams with functionally graded carbon nanotube-reinforced composite face sheets based on a higher-order shear deformation beam theory", *Mech. Adv. Mater. Struct.*, **24**(10), 820-829.
Ebrahimi, F., Ghasemi, F. and Salari, E. (2016), "Investigating thermal effects on vibration behavior of temperature-dependent compositionally graded Euler beams with porosities", *Meccan.*, **51**(1), 223-249.
Ebrahimi, F. and Heidari, E. (2017), "Surface effects on nonlinear vibration of embedded functionally graded nanoplates via higher order shear deformation plate theory", *Mech. Adv. Mater. Struct.*, 1-29.
Ebrahimi, F. and Hosseini, S.H.S. (2016), "Thermal effects on nonlinear vibration behavior of viscoelastic nanosize plates", *J. Therm. Stress.*, **39**(5), 606-625.
Ebrahimi, F. and Jafari, A. (2016), "A higher-order thermomechanical vibration analysis of temperature-dependent FGM beams with porosities", *J. Eng.*, **2016**.
Ebrahimi, F. and Jafari, A. (2018), "A four-variable refined shear-deformation beam theory for thermo-mechanical vibration analysis of temperature-dependent FGM beams with porosities", *Mech. Adv. Mater. Struct.*, **25**(3), 212-224.
Ebrahimi, F. and Mokhtari, M. (2015), "Transverse vibration analysis of rotating porous beam with functionally graded microstructure using the differential transform method", *J. Brazil. Soc. Mech. Sci. Eng.*, **37**(4), 1435-1444.
Ebrahimi, F. and Salari, E. (2015), "A semi-analytical method for vibrational and buckling analysis of functionally graded nanobeams considering the physical neutral axis position", *CMES: Comput. Model. Eng. Sci*, **105**(2), 151-181.
Ebrahimi, F. and Salari, E. (2015), "Size-dependent thermo-electrical buckling analysis of functionally graded piezoelectric nanobeams", *Smart Mater. Struct.*, **24**(12), 125007.
Ebrahimi, F. and Salari, E. (2016), "Effect of various thermal loadings on buckling and vibrational characteristics of nonlocal temperature-dependent functionally graded nanobeams", *Mech. Adv. Mater. Struct.*, **23**(12), 1379-1397.
Ebrahimi, F., Salari, E. and Hosseini, S.A.H. (2015), "Thermomechanical vibration behavior of FG nanobeams subjected to linear and non-linear temperature distributions", *J. Therm. Stress.*, **38**(12), 1360-1386.
Ebrahimi, F. and Zia, M. (2015), "Large amplitude nonlinear vibration analysis of functionally graded Timoshenko beams with porosities", *Acta Astronaut.*, **116**, 117-125.
Eringen, A.C. (1983), "On differential equations of nonlocal elasticity and solutions of screw dislocation and surface waves", *J. Appl. Phys.*, **54**(9), 4703-4710.
Farajpour, A., Hairi Yazdi, M.R., Rastgoo, A., Loghmani, M. and Mohammadi, M. (2016), "Nonlocal nonlinear plate model for large amplitude vibration of magneto-electro-elastic nanoplates", *Compos. Struct.*, **140**, 323-336.
Fischer, L., Wright, V., Guthy, C., Yang, N., McDermott, M., Buriak, J. and Evoy, S. (2008), "Specific detection of proteins using nanomechanical resonators", *Sens. Actuat. B: Chem.*, **134**(2), 613-617.
Fu, Y., Du, H., Huang, W., Zhang, S. and Hu, M. (2004), "TiNi-based thin films in MEMS applications: A review", *Sens. Actuat. A: Phys.*, **112**(2-3), 395-408.
Hadi, A., Nejad, M.Z. and Hosseini, M. (2018), "Vibrations of three-dimensionally graded nanobeams", *Int. J. Eng. Sci.*, **128**, 12-23.
Hadi, A., Nejad, M.Z., Rastgoo, A. and Hosseini, M. (2018), "Buckling analysis of FGM Euler-Bernoulli nano-beams with 3D-varying properties based on consistent couple-stress theory", *Steel Compos. Struct.*, **26**(6), 663-672.
Hosseini-Hashemi, S. and Khaniki, H.B. (2018), "Three dimensional dynamic response of functionally graded nanoplates under a moving load", *Struct. Eng. Mech.*, **66**(2), 249-262.
Hosseini, M., Hadi, A., Malekshahi, A. and Shishesaz, M. (2018), "A review of size-dependent elasticity for nanostructures", *J. Comput. Appl. Mech.*, **49**(1), 197-211.
Hwang, K.S., Lee, J.H., Park, J., Yoon, D.S., Park, J.H. and Kim, T.S. (2004), "In-situ quantitative analysis of a prostate-specific antigen (PSA) using a nanomechanical PZT cantilever", *Lab Chip*, **4**(6), 547-552.
Ilic, B., Yang, Y., Aubin, K., Reichenbach, R., Krylov, S. and Craighead, H. (2005), "Enumeration of DNA molecules bound to a nanomechanical oscillator", *Nano Lett.*, **5**(5), 925-929.
Ilic, B., Yang, Y. and Craighead, H. (2004), "Virus detection using nanoelectromechanical devices", *Appl. Phys. Lett.*, **85**(13), 2604-2606.
Lima, L.M., Fu, W., Jiang, L., Kros, A. and Schneider, G.F. (2016), "Graphene-stabilized lipid monolayer heterostructures: A novel biomembrane superstructure", *Nanosc*, **8**(44), 18646-18653.
Liu, L., Yang, C., Zhao, K., Li, J. and Wu, H.C. (2013), "Ultrashort single-walled carbon nanotubes in a lipid bilayer as a new nanopore sensor", *Nat. Commun.*, **4**, 2989.
Nejad, M.Z., Hadi, A. and Farajpour, A. (2017), "Consistent couple-stress theory for free vibration analysis of Euler-Bernoulli nano-beams made of arbitrary bi-directional functionally graded materials", *Struct. Eng. Mech.*, **63**(2), 161-169.

Nejad, M.Z., Hadi, A., Rastgoo, A. and Omidvari, A. (2018), "Bending analysis of bi-directional functionally graded Euler-Bernoulli nano-beams using integral form of Eringen's non-local elasticity theory", *Struct. Eng. Mech.*, **67**(4), 417-425.

She, G.L., Ren, Y.R., Yuan, F.G. and Xiao, W.S. (2018), "On vibrations of porous nanotubes", *Int. J. Eng. Sci.*, **125**, 23-35.

She, G.L., Shu, X. and Ren, Y.R. (2017), "Thermal buckling and postbuckling analysis of piezoelectric FGM beams based on high-order shear deformation theory", *J. Therm. Stress.*, **40**(6), 783-797.

She, G.L., Yuan, F.G. and Ren, Y.R. (2017), "Research on nonlinear bending behaviors of FGM infinite cylindrical shallow shells resting on elastic foundations in thermal environments", *Compos. Struct.*, **170**, 111-121.

She, G.L., Yuan, F.G. and Ren, Y.R. (2017), "Thermal buckling and post-buckling analysis of functionally graded beams based on a general higher-order shear deformation theory", *Appl. Math. Model.*, **47**, 340-357.

She, G.L., Yuan, F.G. and Ren, Y.R. (2018), "On wave propagation of porous nanotubes", *Int. J. Eng. Sci.*, **130**, 62-74.

She, G.L., Yuan, F.G., Ren, Y.R., Liu, H.B. and Xiao, W.S. (2018), "Nonlinear bending and vibration analysis of functionally graded porous tubes via a nonlocal strain gradient theory", *Compos. Struct.*, **203**, 614-623.

She, G.L., Yuan, F.G., Ren, Y.R. and Xiao, W.S. (2017), "On buckling and postbuckling behavior of nanotubes", *Int. J. Eng. Sci.*, **121**, 130-142.

Sioh, E.L. (2010), "Functional graded material with nano-structured coating for protection", *Int. J. Mater. Prod. Technol.*, **39**(1-2), 136-147.

Witvrouw, A. and Mehta, A. (2005), "The use of functionally graded poly-SiGe layers for MEMS applications", *Mater. Sci. For.*

Zamani Nejad, M., Jabbari, M. and Hadi, A. (2017), "A review of functionally graded thick cylindrical and conical shells", *J. Comput. Appl. Mech.*, **48**(2), 357-370.

Zhou, X., Moran-Mirabal, J.M., Craighead, H.G. and McEuen, P.L. (2007), "Supported lipid bilayer/carbon nanotube hybrids", *Nat. Nanotechnol.*, **2**, 185.

PL